Chemical Engineering Science 173 (2017) 74–90

Contents lists available at ScienceDirect

Chemical Engineering Science

journal homepage: www.elsevier.com/locate/ces

Influence of solids outlets and the gas inlet design on the generation of a gas-solids rotating fluidized bed in a vortex chamber for different types of particles

Waldo Rosales Trujillo, Juray De Wilde *

Université catholique de Louvain, Materials & Process Engineering (IMAP), Place Sainte Barbe 2, B-1348 Louvain-la-Neuve, Belgium

HIGHLIGHTS

- The particle type determines the optimal vortex chamber design.
- A strong central vortex is essential to prevent fine particle losses via the chimney.
- Solids outlets help maintaining a strong central vortex.
- Sufficiently high velocity gas injection is essential for efficient particle retention.
- Limitations with too strong or too small gas inlet jets are demonstrated.

ARTICLE INFO

Article history:
Received 2 March 2017
Received in revised form 12 July 2017
Accepted 16 July 2017
Available online 19 July 2017

Keywords:
Emerging reactor technology
Unconventional fluidized bed
Vortex chamber: process intensification
Reactor design
Fluidization

ABSTRACT

Two design aspects of vortex chambers for the generation of gas-solids rotating fluidized beds are experimentally studied for different types of particles: the solids outlet(s) and the gas inlets. Efficient solids retention and minimal solids losses via the chimney are aimed at so that the gas and solids residence times can be controlled independently. The importance of a strong vortex in the central particle bed freeboard region is demonstrated. It is shown that separate, well-dimensioned and -positioned solids outlets prevent a significant presence of particles in the freeboard region, increasing the vortex strength in this region. This is found to be particularly important when fluidizing small/light particles. The ratio centrifugal force-to-radial gas-solid drag force that is generated by the gas injection is shown to also have an important impact. Theoretically it is shown that this ratio strongly depends on the particle characteristics and to what extent it can be increased by increasing the gas injection velocity, preferentially by reducing the gas inlet slot size and otherwise the number of gas inlet slots. Experiments with different vortex chambers and particles qualitatively confirm the theoretical expectations, but show that limitations are encountered. A very high gas injection velocity prevents efficient penetration of especially fine/light particles in the gas inlet jets which is detrimental for the transfer of tangential momentum between the gas and the particle bed. Slots smaller than the particle size are also shown to be inefficient, as they generate rotational motion of the particles around their own center of gravity.

1. Introduction

Interest in gas-solid rotating fluidized beds in vortex chambers comes from the process intensification that can be achieved as a result of high-G and eventually multi-zone operation. These open perspectives for both significantly reducing equipment size and developing novel processing routes. The former was numerically demonstrated by Trujillo and De Wilde (2010, 2012) for fluid catalytic cracking (FCC), by Staudt et al. (2011) and Ashcraft et al. (2012) for biomass pyrolysis/gasification, and by Ashcraft et al. (2013) for the simultaneous adsorption of SO_2 and NOx (SNAP). Experimental demonstrations of size reduction are mainly in the field of drying (Kochetov et al., 1969a, 1969b; Volchkov et al., 1993, 2003; Eliaers and De Wilde, 2013; Eliaers et al., 2015; Pati et al., 2016). A vortex chamber device for the first-stage drying of granular materials was used at the commercial scale for agricultural applications (Volchkov et al., 2003). An example of a novel processing route based on vortex chamber technology was given by Eliaers et al. (2014) who studied the low-temperature wet coating of cohesive particles in a two-zone vortex chamber device.

* Corresponding author.
E-mail address: juray.dewilde@uclouvain.be (J. De Wilde).

http://dx.doi.org/10.1016/j.ces.2017.07.031
0009-2509/

Nomenclature

List of symbols

a_c	centrifugal acceleration [m_r/s^2]
d_p	particle diameter [m]
D	vortex chamber diameter [m_r]
f	frequency [1/s]
f	factor
L	vortex chamber length [m_r]
m	mass [kg]
n	number of gas inlet slots
P	pressure [Pa]
R	radius [m_r]
s	single slot width [m_r]
S	surface area [m_r^2]
t_b	particle bed thickness (radial direction) [m_r]
u	gas velocity (interstitial) [m_r/s]
v	solids velocity (interstitial) [m_r/s]
V	volume [m^3]
β	drag coefficient [$kg/m_r^3/s$]
ε_i	volume fraction phase i [m_i^3/m_r^3]
ρ_i	density phase i [kg_i/m_i^3]
λ	Eq. (11)

Subscripts

b	bed
eff	effective/effectiveness
g	gas phase
i	inner
inj	injection
o	outer
r	radial
r	reactor
renew	renewal
s	solids
t	tangential

High-G operation allowed reducing the effect of the inter-particle van der Waals forces and treating cohesive particles. Recently, the potential of combining high-G intensified gas-solids contacting, gas-solids separation and solids segregation was recognized (De Wilde et al., 2016; Weber et al., 2017; Verma et al., 2017).

The fluid dynamics and design of gas-solid rotating fluidized beds in vortex chambers has been studied by various groups, but is still not fully understood (Kochetov et al., 1969a,b; Anderson et al., 1971, 1972; Lewellen and Stickler, 1972; Folsom, 1974; Smulsky, 1983; Vatistas et al., 1986; Volchkov et al., 1993, 2013; De Wilde and de Broqueville, 2007; 2008a,b; 2010; Sazhin et al., 2008; Dvornikov and Belousov, 2011; Pitsukha et al., 2012; De Wilde et al., 2016; Weber et al., 2017; Verma et al., 2017). The fluid dynamics is complex and shear at the end walls generates differences in rotation speed depending on the axial position. This effect is pronounced in the absence of particles, leading to strong boundary layer flows along the end walls and axial-radial circulation patterns in the chamber (Savino and Keshock, 1965; Volchkov et al., 1993). In the presence of a particle bed, the effect persists, but is dampened (Volchkov et al., 1993; Trujillo and De Wilde, 2011). Controlling the axial motion on top of the rotational motion is interesting in the context of multi-zone operation – see De Wilde (2014) for more details.

An efficient vortex chamber design must essentially guarantee efficient solids retention with minimal solids losses via the chimney. This allows building up a dense and uniform rotating fluidized bed and controlling independently the gas and solids residence times. It requires a centrifugal force that is high compared to the radial gas-solid drag force. When the centrifugal force compensates the pressure drop over the bed – the so-called cyclostrophic balance, a pseudo-fluidized concentrated particle layer can be formed. The bed is then at maximum density and tangentially, but not radially fluidized. As the superficial gas velocity in the radial direction remains smaller than the minimum fluidization velocity of the particles in the generated high-G field, bubbles are typically not formed. In other cases, the force balance is reached with a less dense and radially fluidized bed. meso-scale non-uniformities can then be formed (De Wilde and de Broqueville, 2007; 2008a,b, 2010). The unique flexibility of vortex chamber generated rotating fluidized beds with respect to the gas flow rate results from the counter-acting forces being affected by the gas flow rate in similar ways (De Wilde and de Broqueville, 2008a,b). The minimum fluidization velocity varies as such with the gas flow rate, as explained in de Broqueville and De Wilde (2009), so that a dense pseudo-fluidized rotating fluidized bed can be maintained in a relatively wide gas flow rate range.

The most important design parameters of a vortex chamber are the diameter and length, the chimney diameter and insertion length, the number of gas inlet slots and their size, and the solids inlet and outlet for operation with a rotating fluidized bed. Studying a limited number of vortex chamber designs in the context of granular material drying, Kochetov et al. (1969a) defined recommendations on ratios of dimensions to be respected. Some basic guidelines for slot design and operating conditions were given in Dutta et al. (2010). Considering the feeding of a batch of particles to a vortex chamber, Trujillo and De Wilde (2011) and De Wilde et al. (2016) showed by means of respectively Computational Fluid Dynamics (CFD) and Discrete Particle Method (DPM) simulations, the importance of a strong vortex in the particle bed freeboard region for efficient solids retention. The rotating fluidized bed is in a sense accelerated and stabilized from two sides, from the outer side by the tangential injection of the gas and from the inner side via the formation of a strong vortex. Reducing the chimney diameter was shown to increase the strength of this vortex, but comes at the cost of an increased pressure drop. The latter can eventually be reduced by making use of a dual-chimney design. The present paper focuses on the solids outlets and the gas inlet slot design. An experimental study with different vortex chamber designs and different types of particles was carried out to gain insight in the fluid dynamics and the influence of these design parameters.

2. Theoretical influence of the gas inlet slot design

A theoretical analysis on the influence of the gas inlet slot design is presented assuming a uniform and relatively thin monodisperse rotating fluidized bed. Expressing that the centrifugal force on a particle should be larger than the radial gas-solid drag force:

$$\frac{2\varepsilon_s \rho_s v_t^2}{D} > \beta u_r, \qquad (1)$$

with both left and right hand side in [N/m^3 reactor] and assuming a zero radial particle velocity. Considering a solids volume fraction $\varepsilon_s > 0.2$ and turbulent flow and focusing on the region at a certain distance from the gas inlet slot where the gas flows nearly radially, the drag coefficient can be calculated from (Gidaspow, 1994):

$$\beta = 1.75\varepsilon_g \rho_g u_r / d_p \tag{2}$$

so that Eq. (1) becomes:

$$2\varepsilon_s \rho_s v_t^2 d_p > 1.75\varepsilon_g \rho_g u_r^2 D \tag{3}$$

A relation between the tangential velocity of the particles v_t and the gas injection velocity $u_{t,inj}$ can be derived considering that the tangential momentum of the bed has to be renewed with a certain frequency f_{renew} to compensate for shear and that the tangential momentum injected with the gas is transferred to the particle bed with an effectiveness $f_{t,eff}$:

$$\varepsilon_g \rho_g u_{t,inj}^2 f_{t,eff} \frac{S_{inj}}{V_{reactor}} = \varepsilon_s \rho_s v_t f_{renew} \frac{2t_b}{D} \tag{4}$$

with t_b the particle bed thickness (in the radial direction). Hence:

$$v_t = \left(\frac{\varepsilon_g \rho_g}{\varepsilon_s \rho_s}\right) \cdot \left(\frac{u_{t,inj}^2 f_{t,eff}}{f_{renew}}\right) \cdot \left(\frac{S_{inj}}{V_{reactor}}\right) \cdot \left(\frac{D}{2t_b}\right) \tag{5}$$

With n gas inlet slots of width s:

$$v_t = \left(\frac{\varepsilon_g \rho_g}{\varepsilon_s \rho_s}\right) \cdot \left(\frac{u_{t,inj}^2 f_{t,eff}}{f_{renew}}\right) \cdot \left(\frac{4ns}{\pi D^2}\right) \cdot \left(\frac{D}{2t_b}\right) \tag{6}$$

The radial gas velocity u_r at a certain distance from the gas inlet slots follows from the gas injection velocity $u_{t,inj}$ as:

$$u_r = \frac{n s u_{t,inj}}{\pi D \varepsilon_g} \tag{7}$$

Substituting Eqs. (6) and (7) in Eq. (3) gives:

$$u_{t,inj}^2 > \frac{1.75}{4} \cdot \left(\frac{D}{2d_p}\right) \cdot \left(\frac{\varepsilon_s \rho_s}{\varepsilon_g \rho_g}\right) \cdot \left(\frac{f_{renew}}{f_{t,eff}}\right)^2 \cdot \left(\frac{t_b}{\varepsilon_g}\right)^2 \tag{8}$$

The tangential momentum renewal frequency f_{renew} of the bed depends on the shear with the walls, so that it can be estimated from:

$$f_{renew} = K \cdot \varepsilon_s \rho_s \cdot \frac{v_t}{D^{0.5}} \tag{9}$$

Substituting Eq. (6) into Eq. (9):

$$f_{renew}^2 = \left(\frac{K \varepsilon_g \rho_g}{D^{0.5}}\right) \cdot \left(\frac{4ns}{\pi D^2}\right) \cdot u_{t,inj}^2 f_{t,eff} \tag{10}$$

so that Eq. (8) becomes:

$$\left(\frac{ns}{\pi D}\right) \equiv \lambda < \frac{2 f_{t,eff}}{1.75K} \cdot \left(\frac{d_p}{\varepsilon_s \rho_s}\right) \cdot \left(\frac{\varepsilon_g}{t_b}\right)^2 \cdot D^{0.5} \tag{11}$$

The design parameter λ is the ratio of the total gas inlet surface area and the surface area of the vortex chamber cylinder. Experimental observations and CFD simulations with tracer gas show that in most cases the injected gas rapidly transfers its tangential momentum to the particle bed (De Wilde, 2014) but $f_{t,eff}$ is smaller than one. In particular cases, $f_{t,eff}$ can become particularly small, as will be demonstrated in the experimental study. Note that Eq. (11) is a criterion for the product of the number of slots, n, and the single slot width, s, and not for n or s individually. A more detailed analysis accounting for eventual non-uniformity in the particle bed requires input from CFD simulations.

Eq. (11) learns that in order to retain particles of given properties in a rotating fluidized bed of thickness t_b and solids volume fraction ε_s inside a vortex chamber of diameter D, λ has to be sufficiently small or, in other words, the gas injection velocity for given gas flow rate has to be sufficiently high. Eq. (11) also shows that λ has to be reduced to deal with smaller or denser particles or to generate a denser or thicker bed. Because of shear, a smaller diameter vortex chamber also requires a smaller λ to generate a bed of given particles, thickness and density. The experimental study with different types of particles and vortex chambers that is presented next allows to qualitatively confirm the theoretical influence of the particle properties on the gas inlet slot design requirement. The influence of separate solids outlets on the flow pattern in the particle bed freeboard region and on the solids retention is also experimentally studied.

3. Experimental set-up

A schematic overview of the experimental set-up is shown in Fig. 1a. Air is fed by means of a 45 kW compressor with a capacity of about 800 Nm^3/h at 0.8 bar relative. A combination of a pressure controller on a vent line and a mass flow controller on the air feeding to the vortex chamber, both PID-controlled, is used to control the gas flow rate to the gas distribution chamber surrounding the vortex chamber. Different vortex chambers can be easily installed. The gas leaves the vortex chamber via a central chimney in one of the end walls of the chamber. Solids are fed from a hopper by means of a dosing screw and rotary sealing valve and conveyed to the vortex chamber by means of secondary air. Solids and a small amount of gas leaving via the solids outlets and solids entrained into the main gas outlet (chimney) are separated in cyclones and the solids are recovered in bins. The accumulated mass of solids is measured with electro-balances. To prevent that fluctuations by the gas flow perturb the functioning of the electro-balance connected to the chimney, the solids recovery bin and the electro-balance are inserted in a hermetic tank below the cyclone (Fig. 1b). This allows drastically damping the effect of gas flow related fluctuations on the electro-balance measurements.

Experiments with different vortex chamber designs and different types of particles are reported. The dimensions and characteristics are summarized in Table 1. The vortex chamber length is 0.21 times its diameter, well below the maximum of 0.5 times the vortex chamber diameter recommended by Kochetov et al. (1969a). The chimney diameter is 0.42 times the vortex chamber diameter, within the range of 0.3–0.5 times the vortex chamber diameter reported optimal by Kochetov et al. (1969a). Based on the theoretical considerations dealt with in Section 2, a vortex chamber with a limited number of relatively large slots (24 × 3 mm) and two vortex chambers with a higher number of small slots (36 × 0.5 mm and 36 × 0.2 mm) were tested. The values of λ were respectively 0.096, 0.024 and 0.0096, spanning more than the range studied by Kochetov et al. (1969a). A limited number of experiments with 72 × 0.5 mm and 72 × 0.2 mm vortex chambers were also carried out. Pictures of the vortex chambers focused on in this paper are shown in Fig. 3a. The gas inlet slots were profiled to improve tangential momentum transfer with the solids. Each vortex chamber was operated without separate solids outlets or with 2 or 4 separate solids outlets. The latter are 5 mm holes in the back end plate of the vortex chamber at 1.5 cm from the cylindrical wall and 45° inclined in the particle bed rotation direction (Fig. 2). The 3 types of particles used are 2 and 1 mm HDPE (high density polyethylene, ρ_s = 960 kg/m^3, Geldart D-type) and FCC catalyst with an average particle diameter of 75 μm (ρ_s = 1500 kg/m^3, Geldart A-type). Whereas the size distribution of the 2 and 1 mm HDPE particles is relatively narrow, this is not the case with the FCC catalyst, with a particle size between typically 20 and 150 μm (e.g. Issangya et al., 2016). The gas flow rate was varied between 200 and 350 Nm^3/h, with a small number of experiments at a higher gas flow rate of up to 800 Nm^3/h. Depending on the type of particles used, the solids flow rate was varied between 2 and 50 g/s, allowing to build

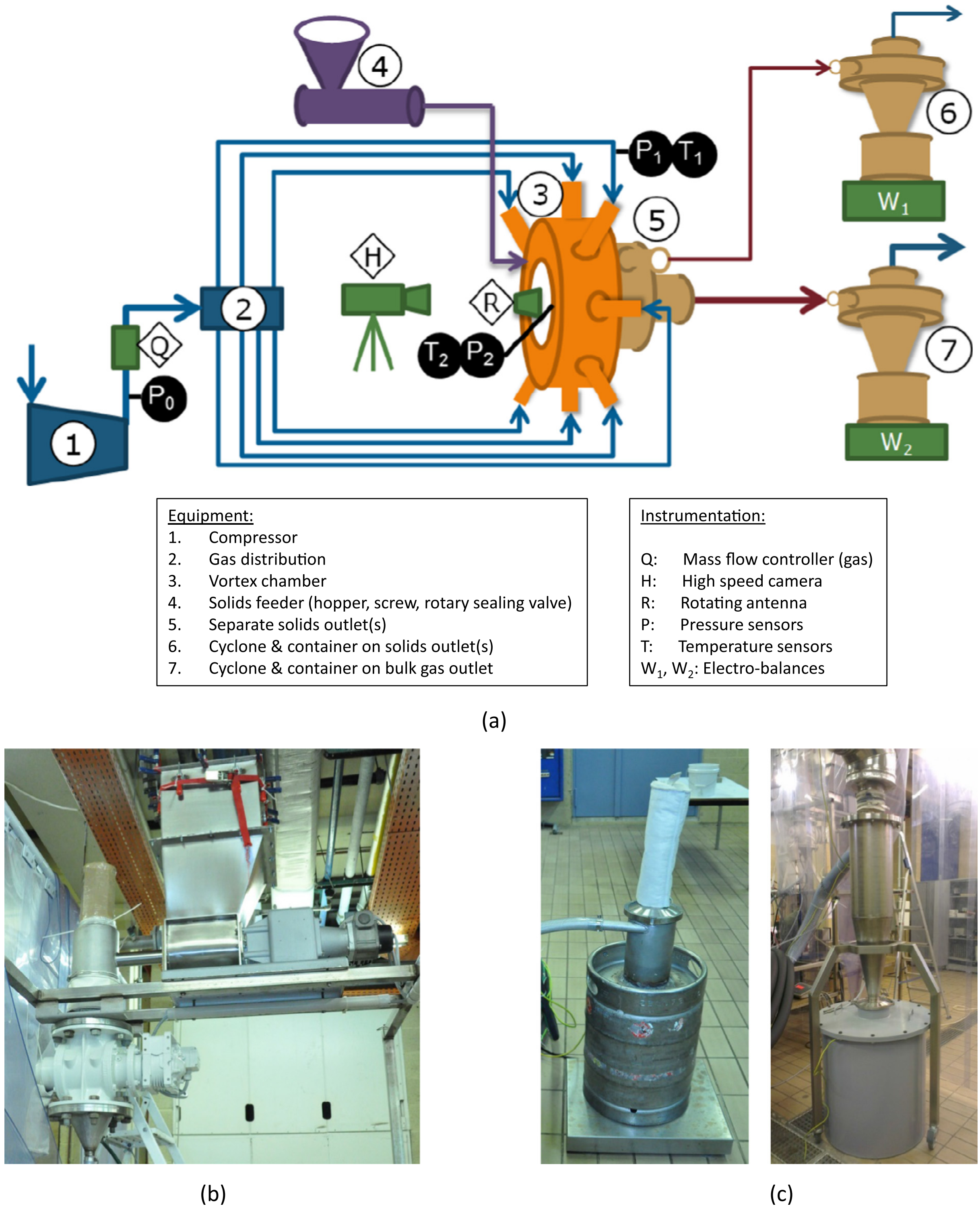

Fig. 1. (a) Schematic overview of the experimental set-up. (b) Solids feeder with screw and rotating sealing valve. (c) Cyclone and bin on electro-balance connected to the solids outlets and cyclone and bin on electro-balance inside a hermetic tank connected to the main gas outlet (chimney).

up a solids loading close to the maximum solids loading of about 1.2 kg for HDPE and 1.9 kg for FCC catalyst particles.

The gas mass flow rate, the solids flow rate and the solids losses via the chimney and solids outlets are measured on-line together with the temperatures, pressure drop over the particle bed and particle bed rotation speed. Electronic temperature and pressure probes are located in the gas distribution chamber and in the chimney region near the center of the vortex chamber. To determine the pressure drop over the particle bed, the pressure drop over the gas inlet slots has to be subtracted from the pressure drop measurement. For each vortex chamber, the pressure drop over the gas inlet slots was measured as a function of the gas flow rate and in the absence of a particle bed (Fig.3b). To avoid an additional pressure drop from the formation of a free vortex during these mea-

Table 1
Experimental vortex chamber dimensions and characteristics.

Vortex chamber	24 × 3 mm	72 × 0.5 mm	36 × 0.5 mm	72 × 0.2 mm	36 × 0.2 mm
Diameter (m)	0.24				
Length (m)	0.05				
Chimney diameter (m)	0.10				
Number of tangential gas inlet slots	24	72	36	72	36
Gas inlet slot size (m)	3×10^{-3}	5×10^{-4}	5×10^{-4}	2×10^{-4}	2×10^{-4}
Fraction of the cylindrical surface taken by gas inlet slots, λ	0.096	0.048	0.024	0.0192	0.0096
Number of separate solids outlets (end wall)	0, 2 or 4				
Solids outlet(s) diameter (m)	5×10^{-3}				
Solids outlet inclination (°)	45° in the particle bed rotation direction				

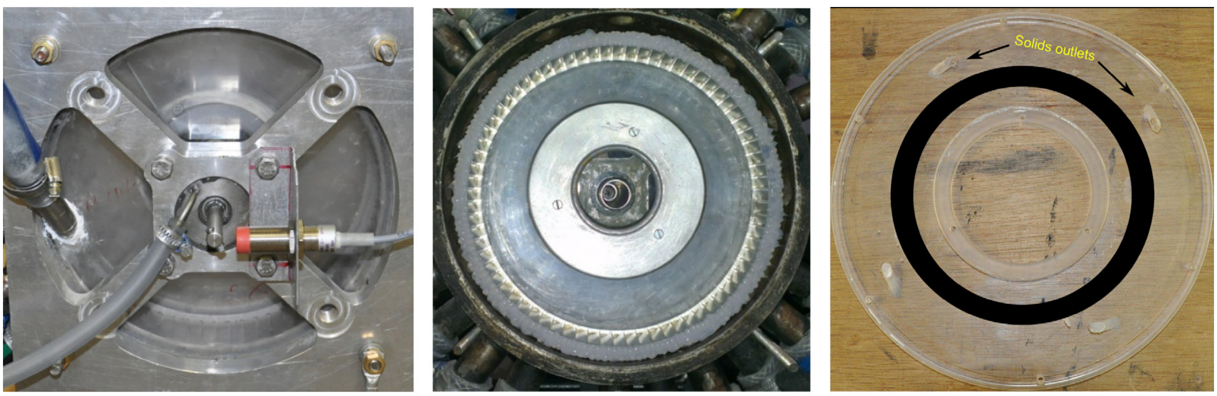

(a) (b) (c)

Fig. 2. (a) Vortex chamber exterior facing the front plate and showing the solids inlet at the left and the rotating antenna axis with detector in the center. (b) Vortex chamber interior facing the front plate with centrally the axis on which the rotating antenna is mounted. (c) Vortex chamber back end plate with centrally the main gas outlet (chimney) and 4 solids inlets, 45° inclined in the particle bed rotation direction.

surements, one of the end plates was removed. The pressure drop over the gas inlet slots has to be sufficiently high to guarantee a uniform distribution of the gas over the different slots and in the axial direction. The data show a behavior that is turbulent in most of the gas flow rate range. The effective slot width during operation can then be estimated from $\Delta P = K \cdot u_{inj}^2$, with K depending on gas properties and the slot length only, and was found to be close to the design target.

The particle bed rotation speed is measured using two techniques, with a rapid digital camera near one of the end walls and with a rotating antenna in the axial center of the bed. Axial differences in rotation speed resulting from shear with the end walls can as such be quantified. The rapid camera takes 500 black and white images at a rate of up to 25,000 frames per second with a resolution of 512-by-256 pixels. The semi-rigid rotating antenna is made of wire and mounted on an axis rotating through two low-friction bearings and linked with a sensor positioned outside the chamber. Two small metal weights (or flags) are fixed to the ends of the rotating antenna, at 3 mm from the cylindrical wall of the vortex chamber. With a sufficiently high solids loading, the rotating antenna is completely immersed in the rotating particle bed. The weights straighten the antenna and increase the drag with the particle bed. Secondary air is injected to keep the bearings clean during operation.

The solids loading in the vortex chamber, m_s, can at any time be estimated by subtracting from the total amount of solids fed to the chamber, the total amount of solids accumulated in the bins connected to the solids outlets and the chimney. Considering the bed height is small compared to the vortex chamber diameter, the hydrostatic pressure drop can then be estimated from the measured solids loading, particle bed rotation speed and particle bed dimensions:

$$\Delta P_{bed,hydrostatic} = \rho_{bed} a_c (R_o - R_i) \quad (12)$$

with:

$$\rho_{bed} = \frac{m_s}{V_{bed}} = \frac{m_s}{\pi (R_o^2 - R_i^2) L} \quad (13)$$

and:

$$a_c = \omega^2 \frac{(R_o + R_i)}{2} = (2\pi f)^2 \frac{(R_o + R_i)}{2}, \quad (14)$$

so that:

$$\Delta P_{bed,hydrostatic} = \frac{2\pi f^2 m_s}{L} \quad (15)$$

A measured pressure drop over the bed smaller than the hydrostatic pressure drop indicates the bed is not or not fully radially fluidized (De Wilde and de Broqueville, 2010; De Wilde, 2014). In case the rotating particle bed is radially fully fluidized, Eq. (15) can also be used to verify the solids loading from the measured pressure drop over the bed and particle bed rotation speed, ω, i.e. assuming that the hydrostatic pressure drop is the dominant contribution to the measured pressure drop over the bed.

Experiments start with feeding air to the vortex chamber at the desired flow rate until the steady state temperature is reached. Solids are then fed at a given rate until a steady state is reached, typically in less than 180 s. The solids feeding is then stopped and measurements continued while the solids loading is slowly decreasing. This allows assuming quasi-steady state operation at any moment and acquiring data at varying solids loading, as verified by doing experiments with different solids loss rates.

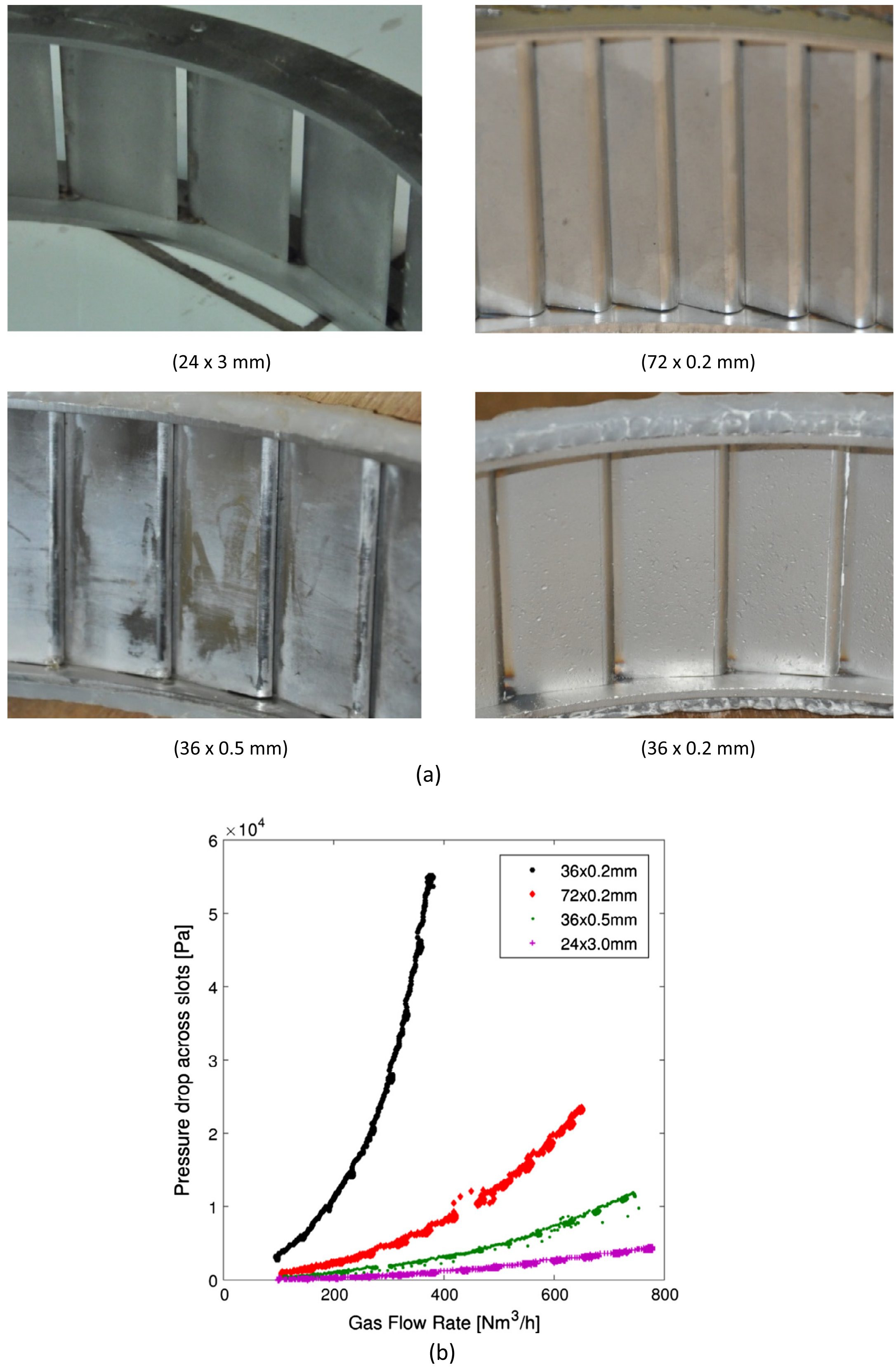

Fig. 3. (a) Different vortex chamber designs. (b) Pressure drop over the gas inlet slots as a function of the gas flow rate for different vortex chambers.

4. Experimental results and discussion

In a first section, the influence of separate solids outlets is focused on. Next, the influence of the gas inlet slot design is studied. The influence of the operating conditions is implicitly dealt with in these sections, but some additional aspects are discussed in a third section.

4.1. Influence of the solids outlet design

Fig. 4 shows for 2 different vortex chambers with respectively 36 × 0.5 mm and 36 × 0.2 mm gas inlet slots and for respectively 2 mm HDPE and 75 μm FCC particles the solids loading in the vortex chamber as a function of the solids flow rate obtained with a gas flow rate of 350 m^3/h and with different solids outlet designs, i.e. with no separate solids outlets – forcing the solids to leave via the chimney – and with 2 and 4 separate solids outlets (see Fig. 2). With the 2 mm HDPE particles, a nearly packed and uniform rotating fluidized bed is formed and the solids concentration in the particle bed freeboard region is low. As the solids loading increases, the bed height increases while the solids concentration in the freeboard region remains low. Solids losses via the chimney occur mainly via the end walls of the vortex chamber where the rotation speed is lower due to friction. Away from the end walls, the centrifugal force is easily large enough to retain the particles in the chamber. Hence, with the 2 mm HDPE particles, maintaining a strong vortex in the freeboard region is not critical and the maximum solids loading for given solids flow rate can be built up in the absence of separate solids outlets. Adding 2 solids outlets reduces the solids loading for given solids flow rate, especially at lower solids flow rate where the maximum solids loading in the chamber is not yet reached. With 4 solids outlets, solids are too efficiently evacuated from the chamber and high solids loadings cannot be reached in the range of solids flow rates studied. The data show that separate solids outlets allow controlling the solids loading in a chamber of given design for given solids flow rate and as such the average solids residence time. Note that the variation of the solids residence time with the solids flow rate is modest and somewhat complex, as the solids loading in the chamber increases also and more or less proportionally with the solids flow rate (Fig. 6). Solids outlets with a control valve can eventually be used.

With respect to the optimal number of solids outlets, a different picture is seen with the 75 μm FCC catalyst. With these smaller/-lighter particles, solids losses through the chimney do not only

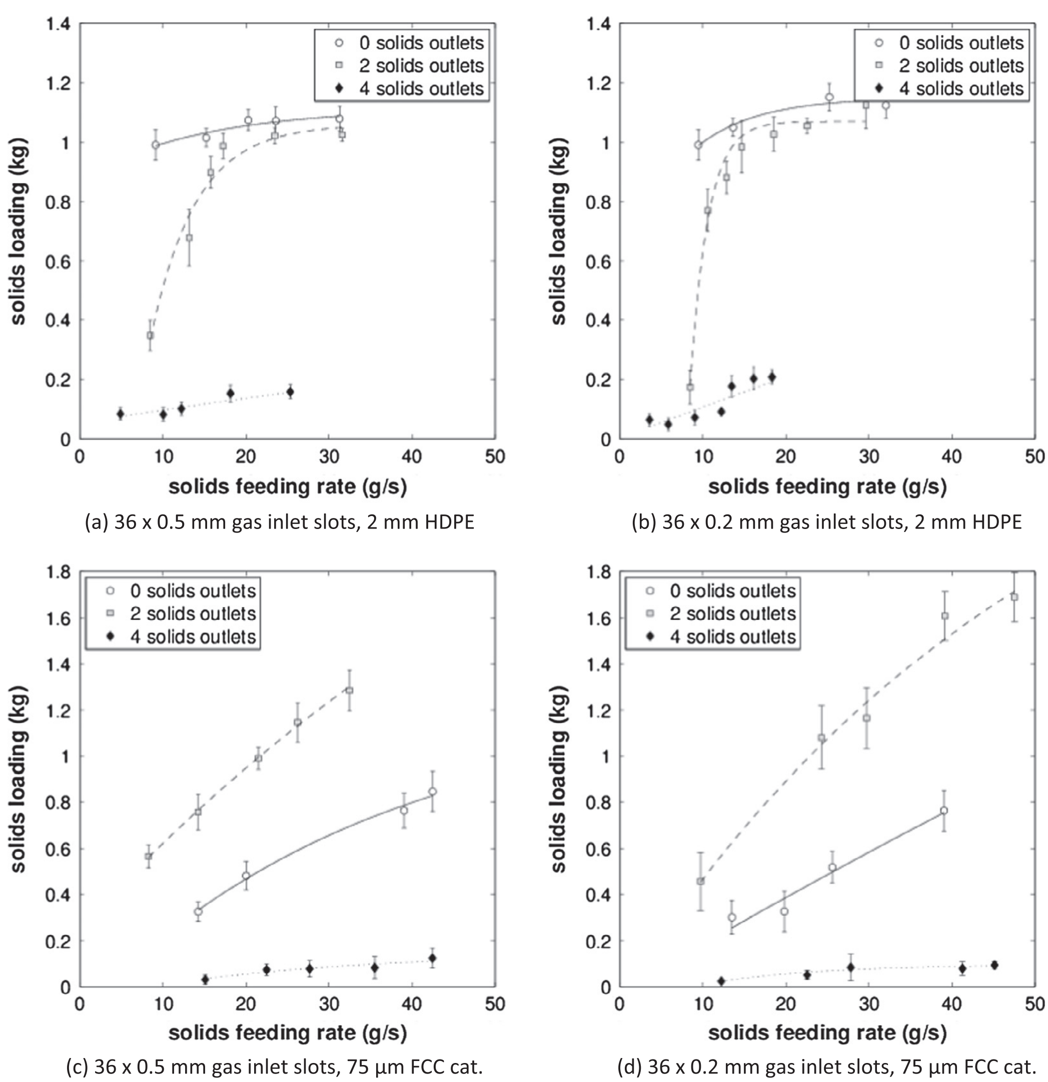

Fig. 4. Solids loading versus solids flow rate for respectively vortex chambers with (a, c) 36 × 0.5 mm and (b, d) 36 × 0.2 mm gas inlet slots and (a, b) 2 mm HDPE and (c, d) 75 μm FCC catalyst particles using different solids outlet designs, i.e. 0, 2 and 4 separate solids outlets (see Figs. 2c and 3a). Gas flow rate of 350 Nm^3/h (36 × 0.2 mm data (b) and (d)). adopted from De Wilde, 2014

proceed via the end walls and a significant presence of particles in the freeboard region is observed, reducing the strength of the vortex in this region. Fig. 4 shows that the use of 2 solids outlets allows evacuating particles from the freeboard region and restoring the vortex strength. For given solids flow rate, a higher solids loading can hence be built up with 2 solids outlets than without solids outlets. With 4 solids outlets, the evacuation of the particles is again over efficient and high solids loadings cannot be built up in the range of solids flow rates applied.

Fig. 5 shows for 3 given solids loadings of 2 mm HDPE particles the particle bed rotation frequency measured by means of the rotating antenna as a function of the gas flow rate for a vortex chamber with 36 × 0.2 mm gas inlet slots equipped or not with separate solids outlets. Both Fig. 5b and c, with a solids loading of 0.5 and 0.8 kg respectively, confirm the positive effect of evacuating solids from the freeboard region via solids outlets on the vortex strength in this region and on the particle bed rotation speed. Fig. 5a at very low solids loading (0.1 kg) provides information on the rotation speed in the freeboard region itself, the rotating antenna not reaching the thin bed. The rotation speed in the freeboard region is seen to be significantly higher than in the particle bed. Furthermore, as particles are evacuated from the freeboard region via solids outlets, the rotation speed in this region is seen to increase drastically. As previously shown (Fig. 4), this has a positive effect on the retention of small/light particles, such as FCC catalyst.

Separate solids outlets in the end walls are seen to have two opposing effects on solids retention. On the one hand, they facilitate evacuation of the particles. On the other hand, they allow enforcing the strength of the vortex in the particle bed freeboard region by evacuating particles from this region. This reduces solids losses via the chimney. Depending on what type of particles is used, one effect is more important than the other to maximize solids retention. For separate control of the gas and solids residence time, one or more separate solids outlet(s) are of course essential.

4.2. Influence of the gas inlet slot design

Fig. 6 shows for 2 different gas flow rates and for respectively 2 mm HDPE, 1mm HDPE and 75 μm FCC particles the solids loading in the vortex chamber as a function of the solids flow rate obtained

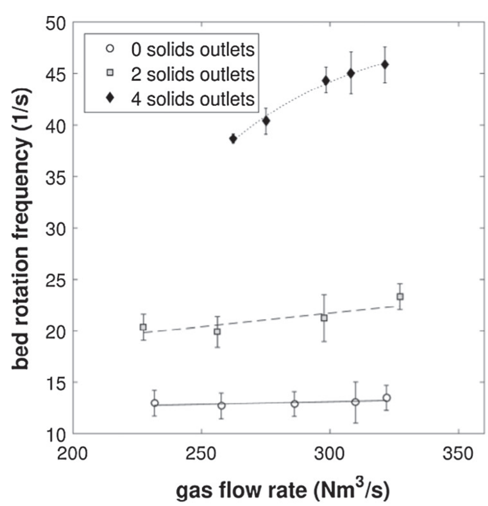

(a) 0.1 kg solids loading

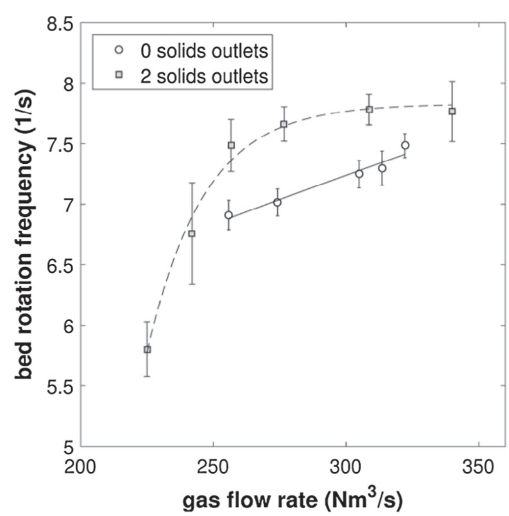

(b) 0.5 kg solids loading

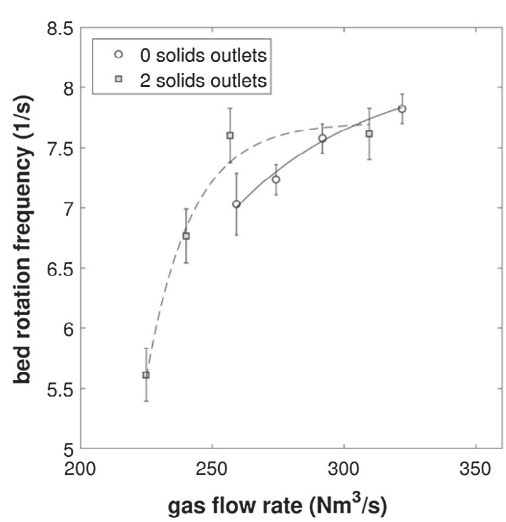

(c) 0.8 kg solids loading

Fig. 5. Rotation speed in the axial center (rotating antenna with flags) versus gas flow rate for a vortex chambers with 36 × 0.2 mm gas inlet slots and 2 mm HDPE particles using different solids outlet designs, i.e. 0 and 2 separate solids outlets (see Figs. 2c and 3a), and for a solids loading of (a) 0.1 kg, (b) 0.5 kg and (c) 0.8 kg.

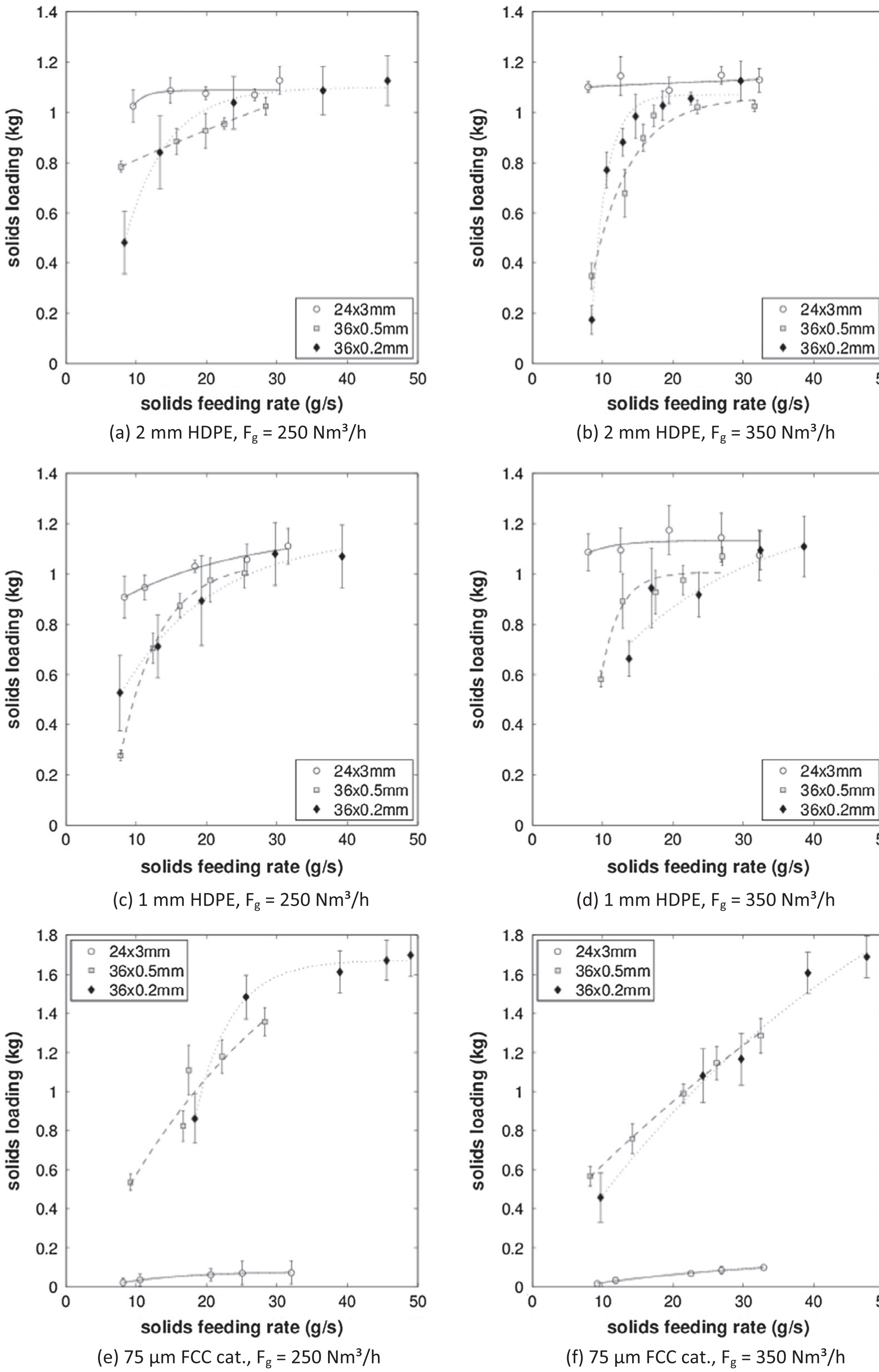

Fig. 6. Solids loading versus solids flow rate with (a, b) 2 mm HDPE, (c, d) 1 mm HDPE and (e, f) 75 μm FCC catalyst particles and a gas flow rate of (a, c, e) 250 Nm^3/h and (b, d, f) 350 Nm^3/h using different vortex chamber designs, i.e. with 24 × 3 mm, 36 × 0.5 mm and 36 × 0.2 mm gas inlet slots, with 2 separate solids outlets (see Fig. 2c and 3a).

with 24 × 3 mm, 36 × 0.5 mm and 36 × 0.2 mm gas inlet slots. Data with 2 separate solids outlets are shown. The solids loading increases typically less than proportionally with the solids flow rate. In the range of operating conditions studied, reaching the maximum solids loading was possible at higher solids flow rate, provided that the vortex chamber was properly designed for the type of particles used.

Fig. 6 shows that the 2 mm HDPE pellets are most efficiently retained in the 24 × 3 mm chamber, despite the large $\lambda = (ns)/(\pi D)$ of 0.096. It demonstrates gas inlet slots sufficiently large compared to the particles are required. A strong gas inlet jet that impacts on part of a particle that is much larger than the jet, such as with the 2 mm particles in the vortex chamber with 0.5 and 0.2 mm slots, generates rotational motion of the particle around its own center of gravity. This reduces the efficiency of tangential momentum transfer between the gas and the bed, $f_{t,eff}$ in Eq. (11). The effect is particularly pronounced at lower solids flow rate/-solids loading where less interactions between particles occur. This explains the poor retention of 1 and 2 mm HDPE particles in the 36×0.5 mm and 36×0.2 mm chambers with pronounced solids losses via the chimney.

With the 75 μm FCC catalyst, solids retention is much more efficient with the 36×0.5 mm and 36×0.2 mm chambers than with the 24×3 mm chamber, as theoretically expected from their lower λ. With the 24×3 mm chamber, the generated centrifugal force is insufficient to build up a dense bed of FCC catalyst particles. With the 36×0.5 mm and 36×0.2 mm chambers, a dense and relatively uniform bed can be built up, although solids losses via the chimney are not completely eliminated. The latter is probably due to the presence of fines that are preferentially lost via the chimney (Weber et al., 2017). Remarkably, the 36×0.5 mm chamber retains the 75 μm FCC catalyst particles better than the 36×0.2 mm chamber at low solids flow rate. This either indicates a difficulty for the particles to penetrate the strong gas inlet jets generated by the 36×0.2 mm chamber or that the momentum transfer between the gas and the particles takes place at a certain distance from a gas inlet slot only. Both lead to a lower value of $f_{t,eff}$ (Eq. (11)). Another explanation is that the particle bed initially builds up in the vicinity of one or both of the end walls where also most of the solids losses via the chimney originate. The near-end wall boundary layer flows are indeed the most pronounced with the 36×0.2 mm chamber, especially at low solids loading. At higher solids flow rate/loading, either of these phenomena will be dampened and the 36×0.2 mm chamber is seen to become slightly more efficient in retaining the 75 μm FCC catalyst particles than the 36×0.5 mm chamber.

Fig. 7 shows camera pictures of the rotating fluidized bed of (a) 1 mm HDPE and (b) 75 μm FCC catalyst obtained in the 24×3 mm vortex chamber at equal solids flow rate, showing the dense and uniform bed obtained with the former and the absence of a bed with the latter. Fig. 7c and d show the bed of 75 μm FCC catalyst obtained with the 36×0.5 mm chamber at two different solids flow rates. Note that the pictures in Fig. 7 were taken at a gas flow rate of 700 Nm^3/h, showing that a bed can be maintained at much higher gas flow rate than quantitatively studied in this work. This can be of interest for applications requiring an extremely low gas phase residence time or high gas throughput. Fig. 8 shows rapid camera snapshots of the bed near one of the end walls with FCC catalyst fed at equal flow rate to a 72×0.5 mm and 36×0.5 mm vortex chamber and illustrates how an increased centrifugal force-to-radial gas-solid drag force ratio increases the solids loading and bed density and improves the bed uniformity.

Axial uniformity was evaluated comparing measurements of the particle bed rotation speed with the rapid camera and the rotating antenna. Differences in rotation speed are much more pronounced with the 75 μm FCC catalyst than with the 1 and 2 mm HDPE particles. Relatively good axial uniformity with mm-sized particles was already observed by Volchkov et al. (1993). Differences in rotation speed as a function of the gas flow rate measured with FCC catalyst fed at 8.35 g/s are shown in Fig. 9, both using the 72×0.5 mm and 36×0.5 mm vortex chamber. The use of the smaller λ 36×0.5 mm vortex chamber slightly improves the axial uniformity, due to the increased pressure drop over the gas inlet slots (Fig. 3b) and the higher solids loading retained in the chamber for the given solids flow rate (Figs. 7 and 8). The significantly lower rotation speed in the near-end wall regions explains most of the

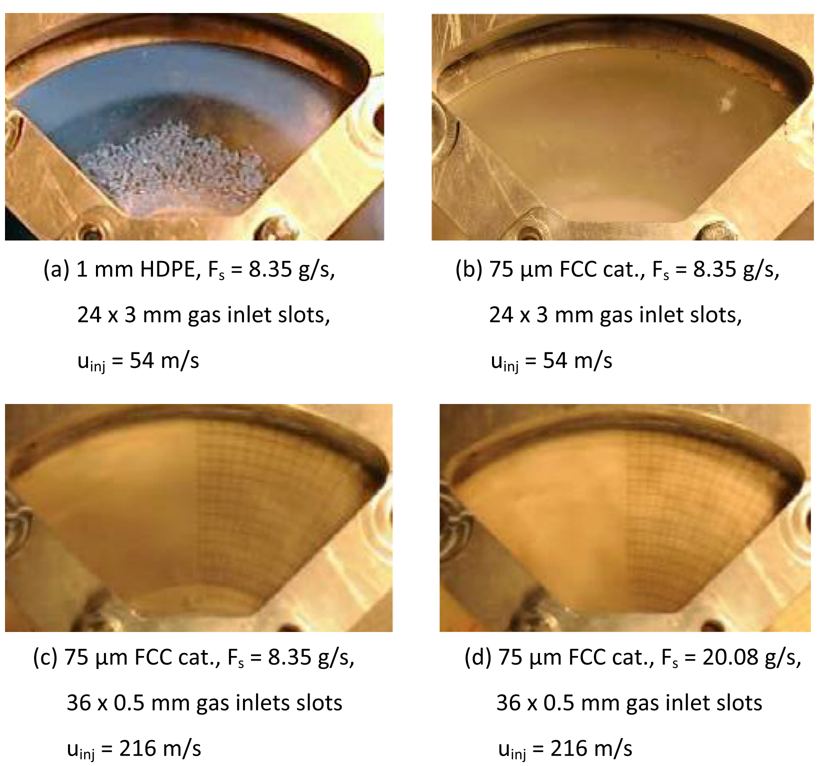

Fig. 7. Rotating fluidized bed of different types of particles in vortex chambers with a different gas inlet slot design. (a, b) 24×3 mm gas inlet slots with (a) 1 mm HDPE, (b) 75 μm FCC catalyst with a solids flow rate of 8.35 g/s. (c, d) 36×0.5 mm gas inlet slots with 75 μm FCC catalyst with a solids flow rate of (c) 8.35 g/s and (d) 20.08 g/s. Gas flow rate of 700 Nm^3/h.

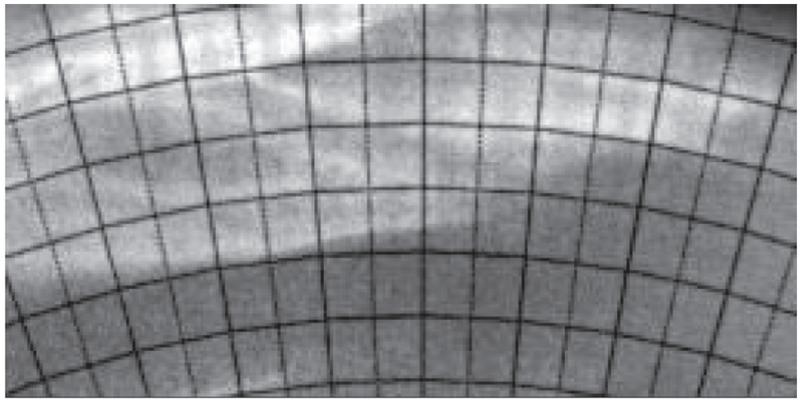

(a) 72 x 0.5 mm gas inlet slots, u_{inj} = 92.5 m/s

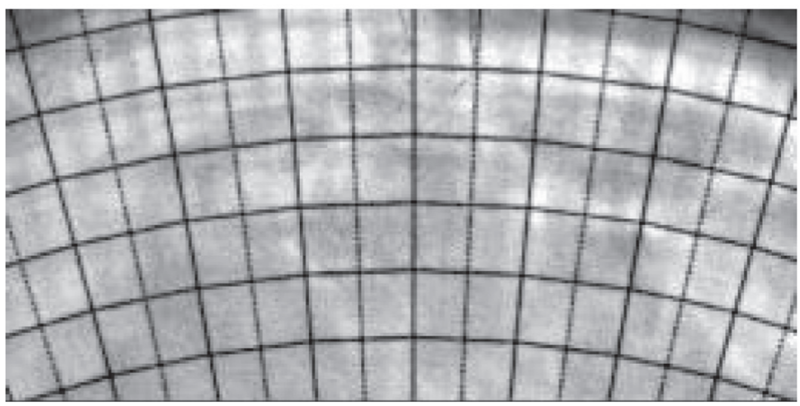

(b) 36 x 0.5 mm gas inlet slots, u_{inj} = 185 m/s

Fig. 8. Rapid camera (1 kHz) snapshots of a rotating fluidized bed of 75 μm FCC catalyst particles in a vortex chamber with (a) 72 × 0.5 mm and (b) 36 × 0.5 mm gas inlet slots at a given gas flow rate of 600 Nm^3/h and solids flow rate of 13.5 g/s.

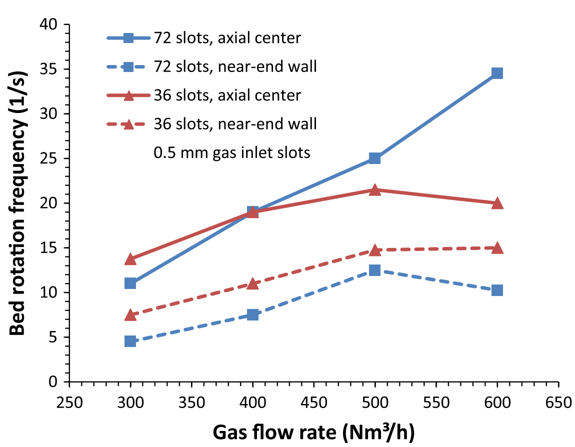

Fig. 9. Rotation speed in the axial center (rotating antenna with flags) and in the near-end wall region (rapid camera) as a function of the gas flow rate when feeding FCC catalyst particles at 8.35 g/s in vortex chambers with 72 × 0.5 mm and 36 × 0.5 mm gas inlet slots. (.) Adapted from De Wilde, 2014

solids losses to the chimney. The strong axial non-uniformity observed in the 72 × 0.5 mm chamber at the higher gas flow rate of 600 Nm^3/h indicates pronounced channeling (De Wilde and de Broqueville, 2007; 2008a,b) with most of the particles rotating in the near-end wall region(s) and only a minor fraction of the particles rotating in the axial center. Under given conditions, a similar observation was made with other chambers. Operation at higher solids loading can significantly reduce/eliminate channeling (De Wilde and de Broqueville, 2008a,b).

The particle bed rotation speed in the axial center of the vortex chamber is further studied in Figs. 10 and 11 that show respectively the bed rotation frequency (1/s) and the static and hydrostatic pressure drop over the bed (kPa) as a function of the solids flow rate and this for different vortex chambers and for (a, b) 2 mm HDPE, (c, d) 1 mm HDPE and (e, f) 75 μm FCC catalyst at gas flow rates of (a, c, e) 250 Nm3/h and (b, d, f) 350 Nm^3/h. The rotating antenna could not be installed in the 24×3 mm chamber. The hydrostatic pressure drop over the bed was derived from the measured solids loading and particle bed rotation speed, see Eqs. (12)–(15). As the solids loading in the chamber increases with increasing solids flow rate (Fig. 6), the bed rotation speed is seen to decrease (Fig. 10). With the 36 × 0.5 mm and 36 × 0.2 mm chambers, the bed rotation speed for given gas and solids flow rates is seen to be lower with the 2 and 1 mm HDPE particles than with the 75 μm FCC catalyst, despite the higher solids loading with the latter (Fig. 6). Furthermore, with the large particles, the rotation speed obtained with the 36 × 0.2 mm chamber is lower than with the 36 × 0.5 mm chamber, despite the higher gas injection velocity with the former. Both observations confirm inefficient transfer of tangential momentum between the injected gas and the bed when using gas inlet slots much smaller than the particles, especially at low solids loading. The decrease of the bed rotation speed with increasing solids flow rate is indeed much less pronounced with the 2 mm and 1 mm HDPE particles (Fig. 10a–d) than with the 75 μm FCC catalyst (Fig. 10e and f), with both the 36 × 0.2 mm and 36 × 0.5 mm vortex chambers. As the solids loading increases with increasing solids flow rate, particles are more densely packed and can less freely rotate around their own center of gravity due to friction with other particles. This increases the

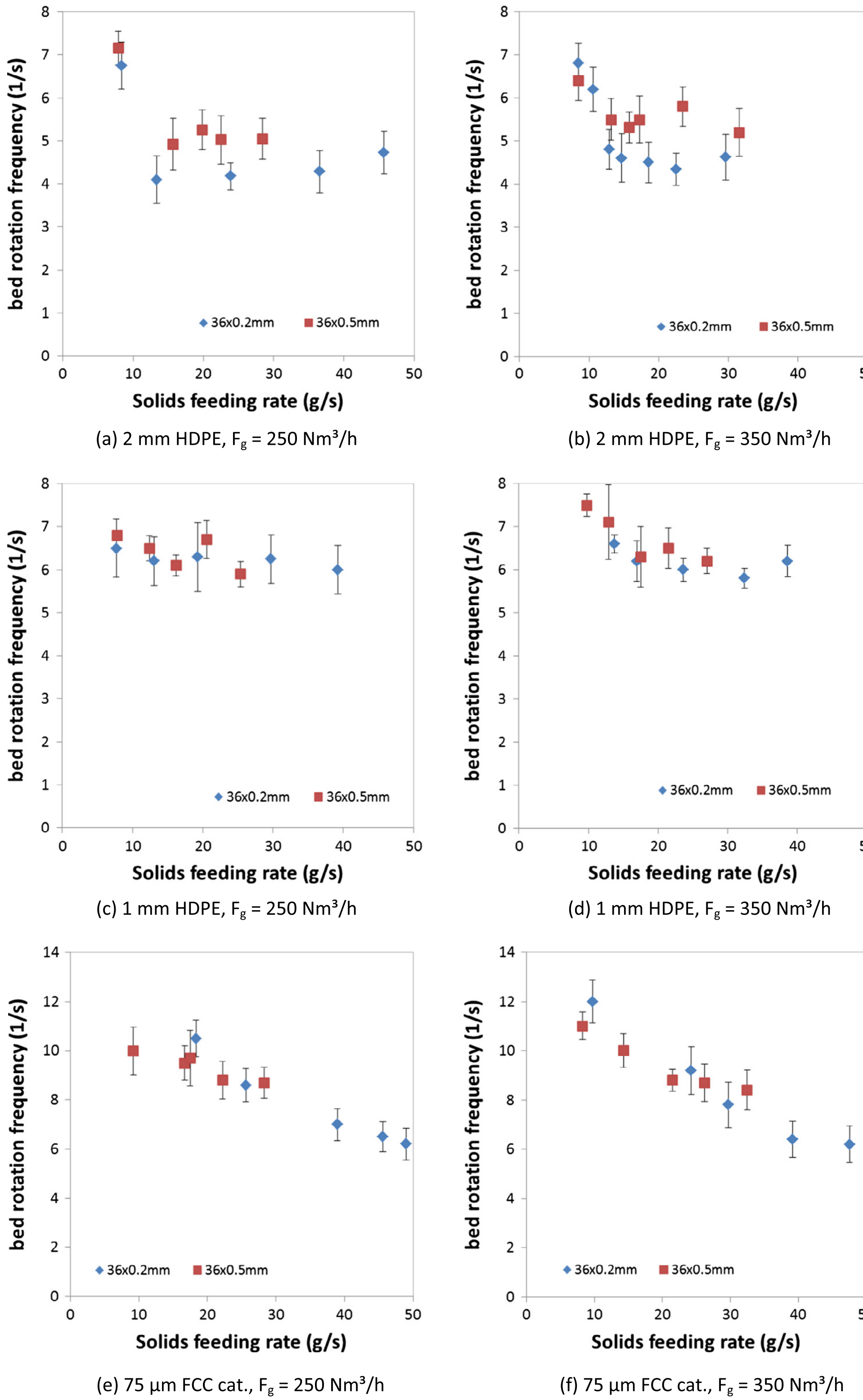

Fig. 10. Rotation speed in the axial center (rotating antenna with flags) versus solids flow rate with (a, b) 2 mm HDPE, (c, d) 1 mm HDPE and (e, f) 75 µm FCC catalyst particles and a gas flow rate of (a, c, e) 250 Nm^3/h and (b, d, f) 350 Nm^3/h using different vortex chamber designs, i.e. with 36 × 0.5 mm and 36 × 0.2 mm gas inlet slots, with 2 separate solids outlets (see Figs. 2c and 3a).

efficiency of tangential momentum transfer between the injected gas and the bed with the 2 mm and 1 mm HDPE particles. The bed rotation speed being lower with the 36 × 0.2 mm than with the 36 × 0.5 mm vortex chamber, also with the 75 µm FCC catalyst (Fig. 10e and f), confirms that particles cannot penetrate the immediate vicinity of too strong gas inlet slots. A certain expansion and deceleration of the injected gas then takes place before actual contact and momentum transfer between gas and particles. The high rotation speed of the antenna in the 36 × 0.2 mm vortex chamber at lower solids flow rate (Fig. 10) is partially due to increased axial

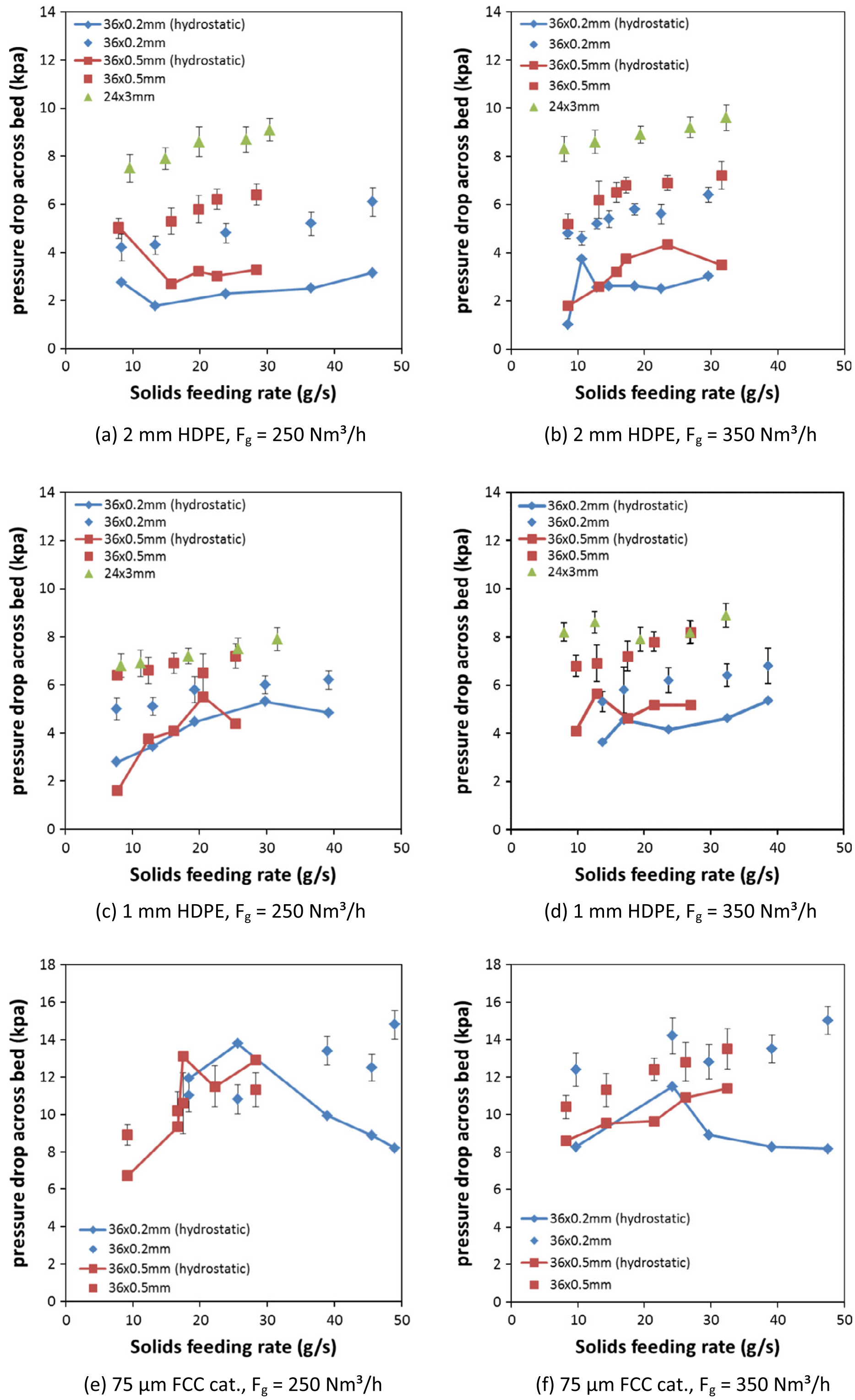

Fig. 11. Particle bed pressure drop versus solids flow rate with (a, b) 2 mm HDPE, (c, d) 1 mm HDPE and (e, f) 75 μm FCC catalyst particles and a gas flow rate of (a, c, e) 250 Nm^3/h and (b, d, f) 350 Nm^3/h using different vortex chamber designs, i.e. with 24 × 3 mm, 36 × 0.5 mm and 36 × 0.2 mm gas inlet slots, with 2 separate solids outlets (see Figs. 2c and 3a).

non-uniformity, with a relatively low fraction of the particles residing in the axial center region of the chamber.

The static and hydrostatic pressure drop over the bed shown in Fig. 11 are affected by both the particle bed rotation speed and the solids loading. Whereas the former decreases with increasing solids flow rate (Fig. 10), the latter increases (Fig. 6), so that the variation of both the static and hydrostatic pressure drop with varying solids flow rate is small. A maximum hydrostatic pressure drop indicates an optimum combination of solids loading and particle bed rotation speed and related centrifugal force. The difference between the static and hydrostatic pressure drop is the result of friction and, to a certain extent, the vortex in the freeboard region. A strong central free vortex was, however, found to improve the bed stability and particle retention and to increase the particle bed rotation speed, so that it also increases the hydrostatic pressure drop. When the bed is radially completely fluidized, the static pressure drop is expected to be larger than the hydrostatic pressure drop. From the friction and chamber efficiency point of view, the difference between the two should be minimal. When using the 36×0.5 mm and 36×0.2 mm vortex chamber, the difference between the static and hydrostatic pressure drop is seen to be the most pronounced with the 2 mm HDPE particles (Fig. 11a and b), somewhat less pronounced with the 1 mm HDPE particles (Fig. 11c and d) and much less pronounced with the 75 μm FCC catalyst (Fig. 11e and f), except at high solids flow rate/solids loading where friction in the rotating bed of FCC catalyst becomes more important, despite the decreasing bed rotation speed (Fig. 10e and f). It is a clear indicator of the efficiency of the given vortex chambers for generating a rotating bed of certain mass of the different particles. Fig. 11 also shows that the difference between the static and hydrostatic pressure drop is slightly more pronounced at higher gas flow rate ($350\ Nm^3/h$, Fig. 11b, d and f compared to $250\ Nm^3/h$, Fig. 11a, c and e), explained by the increased strength of the gas inlet jets and friction. Note that the increased friction at higher solids loading of FCC catalyst may indicate self-rotational motion is also important with small particles. The role of the lift force requires further investigation. Derksen and Larsen (2011) used Lattice-Boltzmann simulations to study drag and lift forces on random, near-wall, mono-, double- and triple layer assemblies of spherical particles in low-Reynolds number shear flow.

With the FCC catalyst, the hydrostatic pressure drop exceeds under certain conditions the measured pressure drop over the bed. As explained in De Wilde and de Broqueville (2008a) and De Wilde (2014), this indicates that the bed is compact and radially not or not fully fluidized. The rotating particle bed is then partially supported by the cylindrical wall of the vortex chamber, and not only by the gas. The pressure drop measurements confirm that the 36×0.2 mm and the 36×0.5 mm vortex chambers are able to generate a dense rotating fluidized bed of FCC catalyst and guarantee a sufficiently high centrifugal force in the axial center region of the vortex chamber. In the near end-wall regions, however, losses to the chimney of especially the finer fraction of FCC catalyst can still occur due to the lower particle bed rotation speed (Fig. 9). Fig. 11 shows that with the 2 mm HDPE particles and to less extent with the 1 mm HDPE particles, the pressure drop over the bed is the highest with the 24×3 mm vortex chamber, followed by the 36×0.5 mm and 36×0.2 mm chambers. This confirms the higher solids loading (Fig. 6) for given gas and solids flow rates when using the 24×3 mm chamber, but also indicates a higher particle bed rotation speed with this chamber due to more efficient momentum transfer between the injected gas and the particle bed. Finally, in the range of gas flow rates shown, the influence of the gas flow rate on the pressure drop over the bed is relatively small in most cases, typical for fully fluidized beds. An increase of the pressure drop with the gas flow rate can be attributed to an increase of the friction with the walls and the strength of the central vortex. The influence of the main operating conditions is discussed in more detail hereafter.

The observed influence of the particle properties on the required gas inlet slot design is in agreement with De Wilde and de Broqueville (2007), who observed a dense and uniform rotating fluidized bed in a 36 cm diameter vortex chamber with 12×4 mm gas inlet slots ($\lambda = 0.0424$) when feeding 2–5 mm HDPE particles, but a less dense and less uniform bed when feeding 300–400 μm alumina. The observations are also in line with Ekatpure et al. (2011) who found that with 70 μm FCC catalyst, no stable bed could be obtained in a 0.54 m diameter vortex chamber with 36×6 mm gas inlet slots ($\lambda = 0.127$), whereas a stable bed was observed with an equal number of 2 mm gas inlet slots ($\lambda = 0.042$). With larger 0.9, 1.6 and 2.4 mm HDPE particles, a stable bed could also be obtained in the 36×6 mm chamber. Anderson et al. (1972) used a vortex chamber with 12×0.3 mm gas inlet slots with λ as small as 0.0038 to fluidize 20 μm talc, 12 μm tungsten and 10 μm zinc particles in a 30.5 cm diameter vortex chamber and reported limited bubbling. No detailed explanations were given on the design choice. Finally, Eliaers et al. (2014) used 72×0.2 mm gas inlet slots in a 24 cm diameter vortex chamber ($\lambda = 0.0191$) for the fluidization and low-temperature wet coating of cohesive 70 μm, $260\ kg/m^3$ Hiprotal whey protein alfa particles. In this case, a centrally installed spray nozzle oriented towards the rotating fluidized bed contributed to minimizing losses of lighter uncoated particles via the chimney, especially the finer fraction. The experimental observations reported in the literature and in this paper qualitatively confirm the theoretical criterion for λ, Eq. (11), but also show a more detailed analysis of the gas inlet slot design may be required, i.e. to address the required number of slots n and single slot width s individually and to account for non-uniformities in the bed and the related value of $f_{t,eff}$ in Eq. (11), e.g. preventing a further reduction of s.

4.3. Influence of the main operating conditions

Fig. 12 illustrates the influence of the gas flow rate on the particle bed rotation frequency (Fig. 12a, c, e) and on the measured pressure drop over the bed (Fig. 12b, d, f), and this for the different particle types and solids loadings of respectively 0.5 kg (Fig. 12a, b), 0.8 kg (Fig. 12c, d) and 1.0 kg (Fig. 12e, f) and using a 36×0.2 mm vortex chamber. Both the bed rotation speed and pressure drop increase less than proportionally with the gas flow rate. The former is explained by increasing shear with the walls with increasing gas flow rate. The effect is more pronounced at lower gas flow rate with FCC catalyst, the bed rotation speed being significantly higher with these particles in the 36×0.2 mm vortex chamber (Fig. 10). As explained in the previous section, in the range of gas flow rates shown in Fig. 12, gas injected at high velocity through the 36×0.2 mm gas inlet slots was seen to pierce partially through the 75 μm FCC catalyst particle bed with actual gas-solid momentum transfer taking place at a certain distance from a gas inlet slot. This explains that the particle bed rotation speed does not increase with increasing gas flow rate with FCC catalyst. Figs. 5 and 6 already showed that the influence of the gas flow rate on the solids loading obtained with given solids flow rate is not very pronounced when operating at (i) sufficiently high gas flow rate to guarantee high-G operation and (ii) sufficiently high solids flow rate or solids loading to ensure a uniform distribution of the gas and particles in the chamber. This is in line with earlier observations by De Wilde and de Broqueville (2008a,b). Fig. 6 showed that the net effect of the gas flow rate on the solids loading for given solids flow rate can be positive or negative, depending on a stronger or weaker effect of the gas flow rate on the radial gas-solid drag force or the centrifugal force. Local phenomena such as shear near the end walls play a crucial role, so that details of the design can have a significant impact on the net effect of the gas flow rate. With FCC catalyst in the 36×0.2 mm chamber and in the given range of operating conditions, the solids loading for given solids flow rate decreases slightly with increasing gas flow rate (Fig. 6). This is due to the bed rotation speed hardly increasing with increasing gas flow rate (Fig. 12a, c, e). Increasing solids losses to the chimney can in particular be expected near the end walls where the particle bed rotation speed is lower (Fig. 9). Fig. 12 shows a clear correlation between the influence of the gas flow rate on the bed rotation speed and the measured pressure drop over the bed. As shown in Fig. 6, the solids loading was not much affected

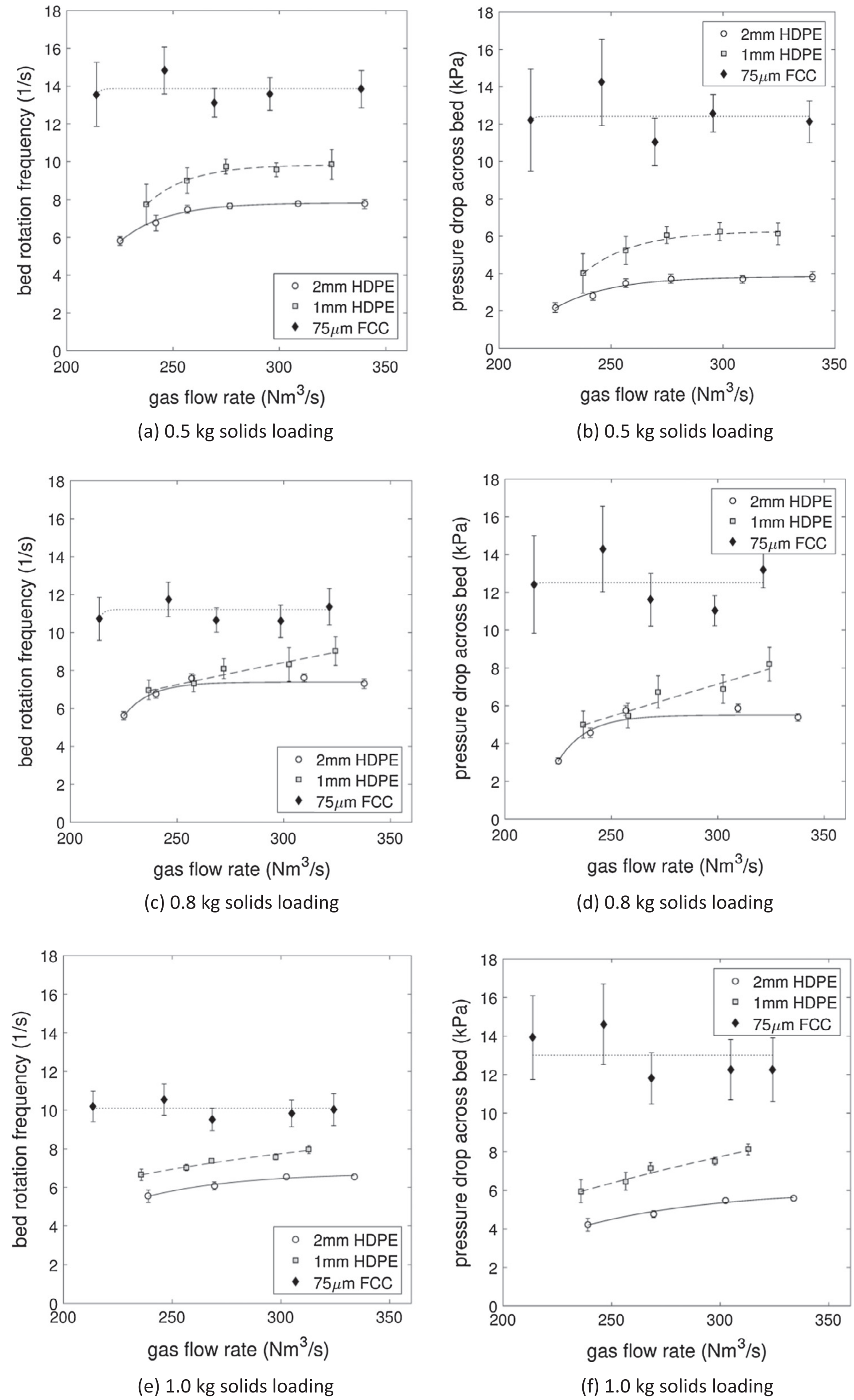

Fig. 12. (a, c, e) Rotation speed in the axial center (rotating antenna with flags) and (b, d, f) pressure drop over the bed versus the gas flow rate with a solids loading of (a, b) 0.5 kg, (c, d) 0.8 kg and (e, f) 1.0 kg of 2 mm HDPE, 1 mm HDPE and 75 µm FCC catalyst using a vortex chamber with 36 × 0.2 mm gas inlet slots, with 2 separate solids outlets (see Fig. 2c and 3a).

by the gas flow rate under the given conditions. A higher bed rotation speed at higher gas flow rate will then indeed result in a higher static pressure drop across the bed, with contributions from the hydrostatic pressure drop, increasing friction with the walls and increasing central vortex strength. The relatively small effect of the gas flow rate on the pressure drop is typical for fully fluidized beds. Note that Fig. 12 clearly illustrates that when using the 36 × 0.2 mm chamber, the transfer of tangential momentum between the injected gas and the particle bed is more efficiently with the 75 µm FCC catalyst than with the 1 and 2 mm HDPE par-

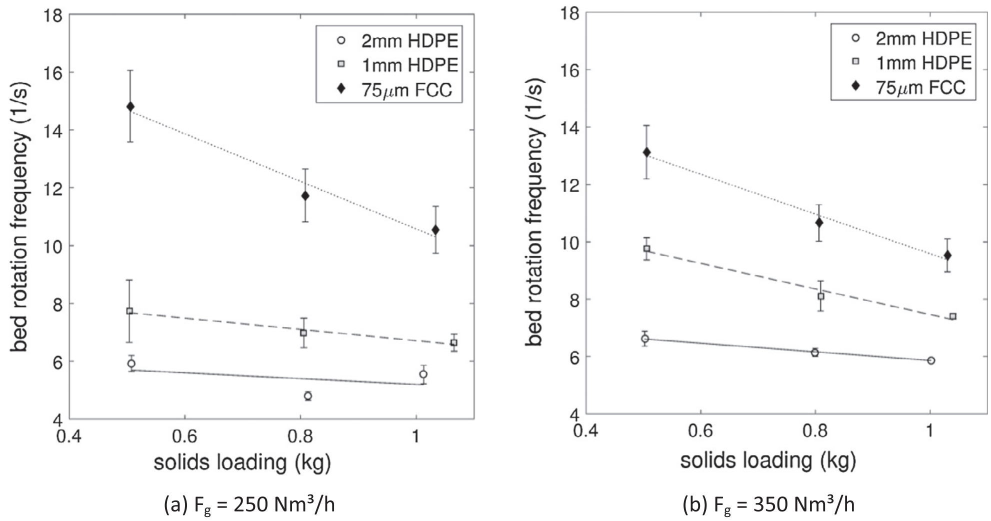

Fig. 13. Rotation speed in the axial center (rotating antenna with flags) versus the solids loading with a gas flow rate of (a) 250 Nm^3/h and (b) 350 Nm^3/h with 2 mm HDPE, 1 mm HDPE and 75 μm FCC catalyst using a vortex chamber with 36 × 0.2 mm gas inlet slots, with 2 separate solids outlets (see Fig. 2c and 3a).

ticles. Especially at low gas flow rate and low solids loading (Fig. 12a, b), the difference in bed rotation speed for given solids loading is pronounced, as discussed earlier.

Fig. 13 shows the influence of the solids loading in the 36 × 0.2 mm vortex chamber on the bed rotation speed in the axial center for as well the 75 μm FCC catalyst and the 1 and 2 mm HDPE particles at a gas flow rate of (a) 250 and (b) 350 Nm^3/h. A similar influence is seen at the two gas flow rates. The particle bed rotation speed logically decreases with increasing solids loading. In the range of operating conditions studied, the decrease is the most pronounced with the 75 μm FCC catalyst and the least pronounced with the 2 mm HDPE particles. This is on the one hand due to the higher particle bed rotation speed with the FCC catalyst and on the other hand due to the improving gas-solid momentum transfer efficiency with increasing solids loading, in particular with the 2 mm HDPE particles in the 36 × 0.2 mm vortex chamber.

5. Conclusions

The influence of the solids outlet(s) and the gas inlet design on the generation of a gas-solid rotating fluidized bed in a vortex chamber was experimentally studied for different types of particles. The generation of a dense and uniform bed and independent control the gas and solids residence times requires efficient solids retention with minimal solids losses via the chimney. The optimal vortex chamber design depends on the type of particles to be fluidized and must ensure the generation of a sufficiently strong centrifugal force. Evacuation of solids from the particle bed freeboard region via well-designed separate solids outlets in one of the end walls helps maintaining a strong vortex in this region. This is seen to drastically improve the solids retention capacity of the vortex chamber, in particular with fine/light particles that are easily entrained into the freeboard region. Injecting the gas at higher velocity by reducing the gas inlet surface area theoretically allows increasing the centrifugal force for given gas flow rate. This is confirmed by the experiments, but limitations are encountered. Too high gas injection velocities may prevent penetration of particularly fine/light particles in the gas inlet jets so that the transfer of tangential momentum between the gas and the particle bed takes place at a certain distance from the gas inlet slots after expansion of the gas. The experiments further show that the use of gas inlet slots smaller than the particles also results in poor transfer of tangential momentum between the gas and the particle bed as the impact of a narrow gas inlet jet on only a portion of a (larger) particle generates rotational motion of the latter around its own center of gravity. When the centrifugal force has to be increased and the slot size cannot be reduced, reducing the number of slots can be considered, although potentially detrimental for the bed uniformity.

Acknowledgements

The authors would like to thank the Fonds de la Recherche Scientifique (FNRS) for the financial support under project FRFC No. 2.4620.11. The authors would like to thank the Fonds européén de développement régional (FEDER) of the European Commission and the Région Wallonne for the financial support under project Flow4Solids (portefeuille Intense4Chem). Axel de Broqueville and Thomas Tourneur are acknowledged for the interesting discussions and their help with understanding the fascinating vortex chamber technology. The authors would like to thank Luc Wautier for his help with the construction of the experimental set-up and for the technical support with the experiments.

References

Anderson, L.A., Hasinger, S., Turman, B.N., 1971. Two Component Vortex Flow Studies, with Implications for the Colloid Core Nuclear Rocket Concept, A.I.A.A. paper, 71, 637.
Anderson, L.A., Hasinger, S.H., Turman, B.N., 1972. Two-component vortex flow studies of the colloid core nuclear rocket. J. Spacecraft 9 (5), 311–317.
Ashcraft, R.W., Heynderickx, G.J., Marin, G.B., 2012. Modeling fast biomass pyrolysis in a gas-solid vortex reactor. Chem. Eng. J. 207 (208), 195–208.
Ashcraft, R.W., Kovacevic, J., Heynderickx, G.J., Marin, G.B., 2013. Assessment of a gas-solid vortex reactor for SO_2/NO_x adsorption from flue gas. Ind. Eng. Chem. Res. 52, 861–875.
de Broqueville, A., De Wilde, J., 2009. Numerical investigation of gas-solid heat transfer in rotating fluidized beds in a static geometry. Chem. Eng. Sci. 64 (6), 1232–1248. http://dx.doi.org/10.1016/j.ces.2008.11.009.
Derksen, J.J., Larsen, R.A., 2011. Drag and lift forces on random assemblies of wall-attached spheres in low-Reynolds-number shear flow. J. Fluid Mech. 673, 548–573.
De Wilde, J., 2014. Gas-solid fluidized beds in vortex chambers. Chem. Eng. Process. 85, 256–290. http://dx.doi.org/10.1016/j.cep.2014.08.013.
De Wilde, J., de Broqueville, A., 2007. Rotating fluidized beds in a static geometry: experimental proof of concept. AIChE J. 53 (4), 793–810. http://dx.doi.org/10.1002/aic.11139.
De Wilde, J., de Broqueville, A., 2008a. Experimental investigation of a rotating fluidized bed in a static geometry. Powder Technol. 183 (3), 426–435. http://dx.doi.org/10.1016/j.powtec.2008.01.024.
De Wilde, J., de Broqueville, A., 2008b. Experimental study of fluidization of 1G-geldart D-type particles in a rotating fluidized bed with a rotating chimney. AIChE J. 54 (8), 2029–2044. http://dx.doi.org/10.1002/aic.11532.

De Wilde, J., de Broqueville, A., 2010. A rotating chimney for compressing rotating fluidized beds. Powder Technol. 199 (1), 87–94. http://dx.doi.org/10.1016/j.powtec.2009.04.017.
De Wilde, J., Richards, G., Benyahia, S., 2016. Qualitative numerical study of simultaneous high-G-intensified gas-solids contact, separation and segregation in a bi-disperse rotating fluidized bed in a vortex chamber. Adv. Powder Technol. 27, 1453–1463.
Dutta, A., Ekatpure, R.P., Heynderickx, G.J., de Broqueville, A., Marin, G.B., 2010. Rotating fluidized bed with a static geometry: guidelines for design and operating conditions. Chem. Eng. Sci. 65 (5), 1678–1693.
Dvornikov, N.A., Belousov, P.P., 2011. Investigation of a fluidized bed in a vortex chamber. J. Appl. Mech. Tech. Phys. 52 (2), 206–211.
Ekatpure, R., Suryawansh, V.U., Heynderickx, G.J., de Broqueville, A., Marin, G.B., 2011. Experimental investigation of a gas-solid rotating bed reactor with static geometry. Chem. Eng. Process. 50 (1), 77–84.
Eliaers, P., De Wilde, J., 2013. Drying of biomass particles: experimental study and comparison of the performance of a conventional fluidized bed and a rotating fluidized bed in a static geometry. Drying Technol. 31 (2), 236–245.
Eliaers, P., de Broqueville, A., Poortinga, A., van Hengstum, T., De Wilde, J., 2014. High-G, low-temperature coating of cohesive particles in a vortex chamber. Powder Technol. 258, 242–251.
Eliaers, P., Pati, J.R., Dutta, S., De Wilde, J., 2015. Modeling and simulation of biomass drying in vortex chambers. Chem. Eng. Sci. 123, 648–664.
Folsom, B.A., 1974. Two-phase Flow in Vertical and Annular Fluidized Beds (PhD thesis). California Institute of Technology.
Gidaspow, D., 1994. Multiphase Flow and Fluidization: Continuum and Kinetic Theory Descriptions. Academic Press.
Issangya, A.S., Karri, S.B.R., Knowlton, T., Cocco, R., 2016. Use of pressure to mitigate gas bypassing in fluidized beds of FCC catalyst particles. Powder Technol. 290, 53–61.
Kochetov, L.M., Sazhin, B.S., Karlik, E.A., 1969a. Experimental determination of the optimal ratios of structural dimensions in the whirl chamber for drying granular materials. Khim. Neft. Mashinostr. 2, 10.
Kochetov, L.M., Sazhin, B.S., Karlik, E.A., 1969b. Hydrodynamics and heat exchange in vortex drying chambers. Khim. Neft. Mashinostr. 9, 10.
Lewellen, W.S., Stickler, D.B., 1972. Two-Phase Vortex Investigation Related to the Colloidal Core Nuclear Reactor, ARL TR 72-0037, Aerospace Research Laboratory, Wright Patterson Air Force Base, OH, USA.
Pati, J.R., Dutta, S., Eliaers, P., Mahanta, P., Chatterjee, P.K., De Wilde, J., 2016. Experimental study of paddy drying in a vortex chamber. Drying Technol. 34 (9), 1073–1084.
Pitsukha, E.A., Teplitskii, Yu.S., Borodulya, V.A., 2012. Investigation of flows in a vortex-bed chamber. J. Eng. Phys. Thermophys. 85 (5), 1025–1033.
Savino, J.M., Keshock, E.G., 1965. Experimental Profiles of Velocity Components and Radial Pressure Distributions in a Vortex Contained in a Short Cylindrical Chamber. NASA Technical Note, NASA TN D-3072, Washington D.C..
Sazhin, B.S., Kochetov, L.M., Belousov, A.S., 2008. Retention capacities and flow patterns of vortex contactors. Theor. Found. Chem. Eng. 42 (2), 125–135.
Smulsky, J.J., 1983. The weighted layer of particles in the cylindrical vortex chamber. J. Appl. Chem. 8, 1782–1789.
Staudt, N., de Broqueville, A., Trujillo, W.R., De Wilde, J., 2011. Low-temperature pyrolysis and gasification of biomass: numerical evaluation of the process intensification potential of rotating- and circulating rotating fluidized beds in a static fluidization chamber. Int. J. Chem. Reactor Eng. 9, paper A43.
Trujillo, W.R., De Wilde, J., 2010. Computational fluid dynamics simulation of fluid catalytic cracking in a rotating fluidized bed in a static geometry. Ind. Eng. Chem. Res. 49 (11), 5288–5298. http://dx.doi.org/10.1021/ie901610f.
Trujillo, W.R., De Wilde, J., 2011. Experimental study of the fluidization of geldart a type catalyst in a rotating fluidized bed in a static geometry, in: 2011 AIChE Annual Meeting, Minneapolis, Minnesota, USA; Oct. 16–21, 2011.
Trujillo, W.R., De Wilde, J., 2012. Fluid catalytic cracking in a rotating fluidized bed in a static geometry: a CFD analysis accounting for the distribution of the catalyst coke content. Powder Technol. 221, 36–46. http://dx.doi.org/10.1016/j.powtec.2011.12.015.
Vatistas, G.H., Lin, S., Kwok, C.K., 1986. Theoretical and experimental studies on vortex chamber flows. AIAA J. 24 (4), 635–642.
Verma, V., Li, T., De Wilde, J., 2017. Coarse-grained discrete particle simulations of particle segregation in rotating fluidized beds in vortex chambers. Powder Technol. 318, 282–292.
Volchkov, E.P., Terekhov, V.I., Kaidanik, A.N., Yadykin, A.N., 1993. Aerodynamics and heat and mass transfer of fluidized particle beds in vortex chambers. Heat Transfer Eng. 14 (3), 36–47.
Volchkov, E.P., Dvornikov, N.A., Yadykin, A.N., 2003. Characteristic features of heat and mass transfer in a fluidized bed in a vortex chamber. Heat Transf. Res. 34 (7&8), 486–498.
Volchkov, E.P., Dvornikov, N.A., Lukashov, V.V., Abdrakhmanov, R.Kh., 2013. Investigation of the flow in the vortex chamber with centrifugal fluidized bed with and without combustion. Thermophys. Aeromech. 20 (6), 663–668.
Weber, J.M., Stehle, R.C., Breault, R.W., De Wilde, J., 2017. Experimental study of the application of rotating fluidized beds to particle separation. Powder Technol. 316, 123–130.